



This is a repository copy of *A Mode-Matching Technique for Analysis of Scattering by Periodic Comb Surfaces*.

White Rose Research Online URL for this paper:
<http://eprints.whiterose.ac.uk/90832/>

Version: Accepted Version

Article:

Valtr, P., Davenport, C.J., Pechac, P. et al. (1 more author) (2015) A Mode-Matching Technique for Analysis of Scattering by Periodic Comb Surfaces. *IEEE Transactions on Antennas and Propagation*, 63 (9). 4016 - 4023. ISSN 0018-926X

<https://doi.org/10.1109/TAP.2015.2452945>

Reuse

Unless indicated otherwise, fulltext items are protected by copyright with all rights reserved. The copyright exception in section 29 of the Copyright, Designs and Patents Act 1988 allows the making of a single copy solely for the purpose of non-commercial research or private study within the limits of fair dealing. The publisher or other rights-holder may allow further reproduction and re-use of this version - refer to the White Rose Research Online record for this item. Where records identify the publisher as the copyright holder, users can verify any specific terms of use on the publisher's website.

Takedown

If you consider content in White Rose Research Online to be in breach of UK law, please notify us by emailing eprints@whiterose.ac.uk including the URL of the record and the reason for the withdrawal request.



eprints@whiterose.ac.uk
<https://eprints.whiterose.ac.uk/>

A Mode Matching Technique for Analysis of Scattering by Periodic Comb Surfaces

Pavel Valtr, Christopher J. Davenport, Pavel Pechac, Senior Member, IEEE, and Jonathan M. Rigelsford, Senior Member, IEEE

Abstract—Numerical techniques for calculating electromagnetic fields within three dimensional surfaces are computationally intensive. Therefore, this paper presents the application of a mode-matching technique developed for analyzing electromagnetic scattering from periodic comb surfaces illuminated by a plane wave. A set of linear equations have been developed to calculate mode coefficients of the field distribution for both E-polarized and H-polarized incident waves. Analysis is performed for two cases where the comb thickness is either infinitely thin or of a finite thickness. The technique is shown to accurately predict both field intensities within the near-field of the periodic surface and far-field scattering patterns. Results are compared to those obtained using the finite integration techniques (FIT) implemented in CST Microwave Studio. Furthermore, numerical results are compared to measurements of an aluminum prototype. Additional far-field scattering measurements using a bi-static system provide additional confidence in CST simulations and the mode-matching methods presented here.

Index Terms—Mode matching, electromagnetic scattering, periodic structures, CST Microwave Studio.

I. INTRODUCTION

THE use of periodic structures and surfaces to control scattering of electromagnetic waves has been comprehensively investigated. Their use in both indoor and outdoor environments have been explored. Typical examples include using periodic comb surfaces for reducing the interference caused by an Instrument Landing System (ILS) at airports [1]. Alternatively, corrugated surfaces can be used to improve signal coverage close to a building due to surface wave propagation [2]. The control of propagation in indoor environments was described in [3], where various periodic structures can reduce the specular scatter down corridors. By suppressing interference between adjacent co-channel Wi-Fi access points, signal coverage can be improved [4].

Manuscript received 18th November, 2014. This work was supported by FP7 Marie Curie IAPP project No. 286333 WiFEEB - Wireless Friendly Energy Efficient Buildings.

P. Valtr and P. Pechac are with the Department of Electromagnetic Field, Faculty of Electrical Engineering, Czech Technical University in Prague, Technicka 2, 166 27 Prague 6, Czech Republic (e-mail: Pavel.Valtr@fel.cvut.cz, pechac@fel.cvut.cz).

C.J. Davenport and J.M. Rigelsford are with the Department of Electronic & Electrical Engineering at The University of Sheffield, Sir Frederick Mappin Building, Mappin Street, Sheffield, S1 3JD, UK (e-mail: christopher.davenport@sheffield.ac.uk, j.m.rigelsford@sheffield.ac.uk)

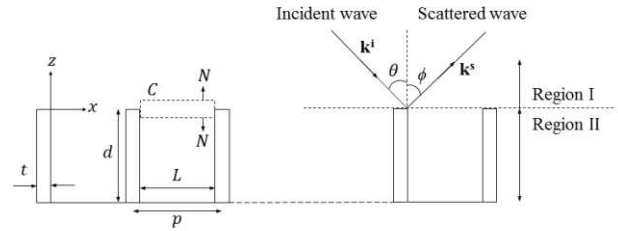


Fig. 1. Geometry of the corrugated surface problem.

Mathematically, the scattering properties of periodic comb surfaces were studied by several authors [5, 6]. In [7], a mode matching technique was applied to scattering by an inclined strip grating and in [8] this method was used to arrive at simple approximate closed-form formulas for mode coefficients of a parallel-plate waveguide. In this work we apply mode-matching technique to solve the problem of scattering by a comb grating structure. Analytical solutions have been applied to many different periodic structures, such as sinusoidal [9], saw-shaped [10], and comb [11] gratings. A comparison of different methods is described in [12], with the scattering from a sinusoid considered with use of the Masel, Merrill, and Miller (MMM) method [13], the Modified Physical Optics (MPO) method [14], and Waterman's Plane Harmonics (WPH) [15] method all discussed. Mode matching methods have been investigated in [16], where the analysis is based on Green's second theorem, describing the integration around a closed contour. Various periodic structures such as high impedance surfaces (HIS) are analyzed using the mode matching analysis in [17].

In this paper, we present a mode-matching solution to the scattering and fields within a periodic comb surfaces, reinforced by CST simulations and experimental measurement of an aluminum surface. Building on the work referenced above, we present analytical solutions for calculating the electric field within or above a comb surface. Equations are developed for both TE and TM polarizations and can be applied to combs having any finite thickness. This enables computationally fast analysis of periodic scattering surfaces.

Section II introduces the use of Floquet scattering modes in combination with waveguide cavity theory to calculate field distribution of a periodic comb structure. Section III provides a generic field matching solution, whereby the thickness of the fins does not affect the analytical solution, to calculate the

respective field at a certain position on the structure. Section IV uses the electric field calculation for infinitely thin fins ($t=0$) to calculate the far-field scattering pattern of the structure. These analytical results are verified using CST simulations. Section V expands on the field calculation to consider when there is a finite thickness to the fins ($t>0$). Once again, CST simulations are produced to compare to our analytical results. Section VI uses experimental measurements and further CST simulations to further verify the analytical work presented in this paper. The paper is concluded in Section VII.

II. ANALYTICAL FORMULATION

In this section we present the analytical formulation of the equations required to calculate the electromagnetic fields within a periodic comb surface. A two-dimensional geometry of the periodic surface and incident wave is shown in Fig. 1. The structure consists of perfectly conducting periodic fins of thickness t on a ground plane. In contrast to previous research [17], this work considers surfaces which are electrically large in terms of the wavelength of the illuminating source. The period and height of the fins are denoted by p and d , respectively. The inner distance between the fins is L , where $L = p - t$. Mathematically, the problem is split into two different regions, where the field is calculated by different equations. Region I is positioned above the structure at $z>0$. Region II occurs in the structure itself, at distance $-d<z<0$. These regions are labelled as I and II (see Fig. 1).

The electromagnetic plane wave illuminating the periodic surface, is represented by the vector \mathbf{k}^i and is incident in Region I at an angle, θ and is reflected (as specular scatter) at an angle, ϕ . The angles θ and ϕ are positive when the x -component of \mathbf{k}^i and \mathbf{k}^s are respectively in the positive direction of x -axis. The scattering scenario is treated as a two-dimensional problem within the x - z plane.

Using the time harmonic phasor form ($e^{j\omega t}$) of an incident plane wave illuminating the surface expressed as:

$$e^{-j(\alpha_0 x - \beta_0 z)} \quad (1)$$

the resulting wave is scattered from the periodic surface and can be expressed as the summation of spatial harmonics based on Floquet theory [18], namely:

$$\sum_{m=-\infty}^{\infty} A_m e^{-j(\alpha_m x + \beta_m z)} \quad (2)$$

Then the total field in Region I, representing the y -component of electric or magnetic field intensity in the case of a TE or TM polarized incident wave, can therefore be expressed as:

$$\psi^I = e^{-j(\alpha_0 x - \beta_0 z)} + \sum_{m=-\infty}^{\infty} A_m e^{-j(\alpha_m x + \beta_m z)} \quad (3)$$

Where unitary amplitude of incident wave is assumed, k_0 is the wave number, and where α and β are x and z components of \mathbf{k}_0 , respectively.

$$\alpha_m = \alpha_0 + \frac{2\pi m}{p} \quad (4a)$$

$$\beta_m = \sqrt{k_0^2 - \alpha_m^2} \quad (4b)$$

and

$$\alpha_0 = k_0 \sin \theta \quad (4c)$$

Due to the electrically large size of the features of the periodic surface, the total field in Region II can therefore be written as a summation of forward-travelling and reflected wave within a waveguide cavity as:

$$\psi_{TE}^{II} = \sum_{m=1}^{\infty} B_m \sin \frac{m\pi x}{L} [e^{jk_m z} - e^{-jk_m(2d+z)}] \quad (5a)$$

in the case of TE-polarized incident wave and as

$$\psi_{TM}^{II} = \sum_{m=0}^{\infty} B_m \cos \frac{m\pi x}{L} [e^{jk_m z} + e^{-jk_m(2d+z)}] \quad (5b)$$

in the case of TM-polarized incident wave. Where the imaginary part of k_m must be negative to ensure wave attenuation along the z -axis:

$$k_m = \sqrt{k_0^2 - \left(\frac{m\pi}{L}\right)^2} \quad (6)$$

Equation 2a and 2b enable us to develop a series of analytical formula described in the following sections of this paper.

III. GENERIC FIELD MATCHING SOLUTION FOR FINS OF ARBITRARY THICKNESS

In this section we develop a generic field matching solution for the periodic surface illustrated in Fig. 1 comprising of fins of arbitrary thickness. Such a solution enables us to predict the field distribution within or near to an infinite periodic structure. The validity of the theory is assumed for structures with a finite number of fins as well.

Firstly this has been achieved by developing the work published in [7, 8] to utilize Green's second theorem [19] in order to match fields ψ^I and ψ^{II} . By selecting the integration path intersecting regions I and II, thus relating both fields in one equation. Therefore Green's second theorem can be expressed in the form

$$\oint_C \left(\phi \frac{\partial \psi}{\partial N} - \psi \frac{\partial \phi}{\partial N} \right) dl = \iint_S (\phi \nabla^2 \psi - \psi \nabla^2 \phi) ds \quad (7)$$

where the integration is made along an arbitrary closed curve, C and forms a boundary of surface, S. The curve C is represented by its outer normal, N. The function ϕ is an auxiliary function; in the case where ϕ satisfies Helmholtz equation, the right side of (7) is equal to zero. In our case the curve C is chosen as indicated in Fig. 1, where the integration is completed over one period of the grating. The contribution to the integral is in both directions of the x-axis only; the contribution in the direction of z-axis is negligible. Assuming ϕ satisfies Helmholtz equation, (7) yields

$$\int_0^L \left(\phi \frac{\partial \psi^I}{\partial z} - \psi^I \frac{\partial \phi}{\partial z} \right) dx + \int_L^0 \left(\phi \frac{\partial \psi^{II}}{\partial z} - \psi^{II} \frac{\partial \phi}{\partial z} \right) dx = 0 \quad (8)$$

In general, ψ^I and ψ^{II} are expressed using an infinite number of coefficients: A_m and B_m , for ψ^I and ψ^{II} respectively. Practically, the number of coefficients is limited as $m = -M, \dots, -1, 0, 1, \dots, M$ in the case of A_m coefficients and $m = 1, 2, \dots, 2M + 1$ in the case of B_m coefficients, resulting in overall number of unknowns in (8) equal to $4M + 2$. Therefore $2M + 1$ of pairs of linearly independent equations are needed to solve for A_m and B_m coefficients. This is achieved by selecting $2M + 1$ linearly independent pairs of ϕ as

$$\phi_n^{+TE} = \sin\left(\frac{n\pi x}{L}\right) e^{-jk_n z} \quad (9a)$$

$$\phi_n^{-TE} = \sin\left(\frac{n\pi x}{L}\right) e^{jk_n z} \quad (9b)$$

for TE polarization where $n = 1, 2, \dots, 2M+1$. Similarly, they can be represented as

$$\phi_n^{+TM} = \cos\left(\frac{n\pi x}{L}\right) e^{-jk_n z} \quad (9c)$$

$$\phi_n^{-TM} = \cos\left(\frac{n\pi x}{L}\right) e^{jk_n z} \quad (9d)$$

for TM polarizations where $n = 0, 1, \dots, 2M$. Inserting (3), (5) and (9) in (8) gives following set of linear equations that are used to calculate A_m and B_m .

$$\sum_{m=-\infty}^{\infty} (\beta_m - k_n) \cdot F_{n,m} A_m + G_n B_n = (\beta_0 + k_n) \cdot F_{n,0} \quad (10a)$$

$$\sum_{m=-\infty}^{\infty} (\beta_m + k_n) \cdot F_{n,m} A_m + G_n' B_n = (\beta_0 - k_n) \cdot F_{n,0} \quad (10b)$$

Where

$$F_{n,m} = \frac{n\pi/L}{(n\pi/L)^2 - \alpha_m^2} [1 - e^{-j\alpha_m L} \cos(n\pi)] \quad \text{for TE pol.} \quad (11a)$$

$$F_{n,m} = \frac{j\alpha_m}{(n\pi/L)^2 - \alpha_m^2} [1 - e^{-j\alpha_m L} \cos(n\pi)] \quad \text{for TM pol.} \quad (11b)$$

and where

$$G_n = k_n L \\ G_n' = k_n L e^{-2jk_n d} \quad \text{for TE pol.}$$

$$G_n = 2k_n L \\ G_n' = -2k_n L e^{-2jk_n d} \quad \text{for TM pol., } n = 0$$

$$G_n = k_n L \\ G_n' = -k_n L e^{-2jk_n d} \quad \text{for TM pol., } n \neq 0$$

The field distribution within or near to the structure is now readily available using (3, 5) with use of A_m and B_m coefficients, that are in turn obtained by solving the set of equations (10). As Region I and Region II have to be identical at the boundary ($z=0$), the number of harmonics in each region must be the same i.e. $2M+1$. This is also necessary for the numerical stability of solving Eq. 10a and 10b. In general, for a given geometry the number of modes considered M , must increase as the frequency of interest increases. For the examples presented in this work $M=19$, although $M=7$ would provide comparable results for frequencies up to 20 GHz.

A. Comparison of analytical simulation with CST for infinitely thin combs

The analytical solution generated in the previous section is compared to the finite integral technique (FIT)-based software CST Microwave Studio [20], in order to verify the theoretical prediction of field distribution by (3, 5) using coefficients obtained by the procedure described earlier in this section. For both the analytical solution and the CST simulation, the tested periodic surface consists of 12 fins separated by a fin period, p of 20 mm. The height d of each fin, d is 50 mm. The width of the structure along the y-axis direction is 400 mm. CST simulations were performed for both the full 3D structure and the representative 2D structure using periodic boundaries as described in [4] which is more computationally efficient.

The magnitude of the y-component of the electric field intensity, E_y for TE, and magnetic field intensity, H_y for TM polarized incident waves are shown in Fig. 2, where $E_y = \psi^I$ and $H_y = \psi^I / Z_0$. The field is calculated with respect to unitary amplitude of incident electric field intensity. The observation point is in the center of the structure at height $z = 20$ mm and -20 mm. The field intensity is shown as a function of frequency for incidence angle $\theta = 50^\circ$. The predicted field outside ($z = 20$ mm) and inside ($z = -20$ mm) the structure are shown in Fig. 2 and Fig. 3 respectively. The results show that there is excellent agreement between the mode-matching approach described previously, and the fully numerical solution obtained by CST.

It can be observed that the CST simulation result for 2D and 3D cases are almost identical.

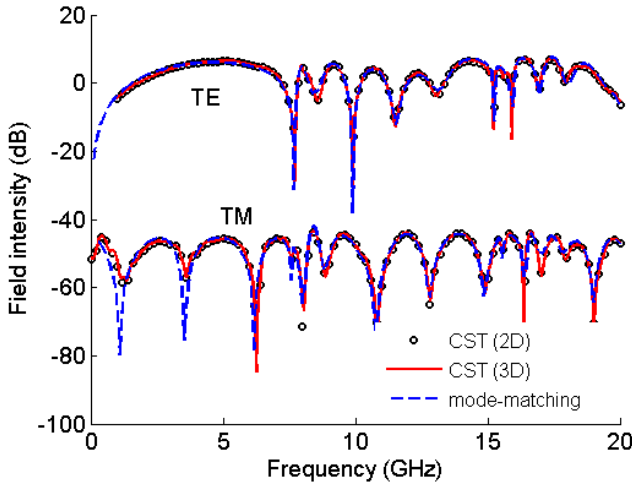


Fig. 2. Comparison of modelling results; considering the field outside the structure at $[x; y; z] = [11 \text{ cm}; 0 \text{ cm}; 2 \text{ cm}]$.

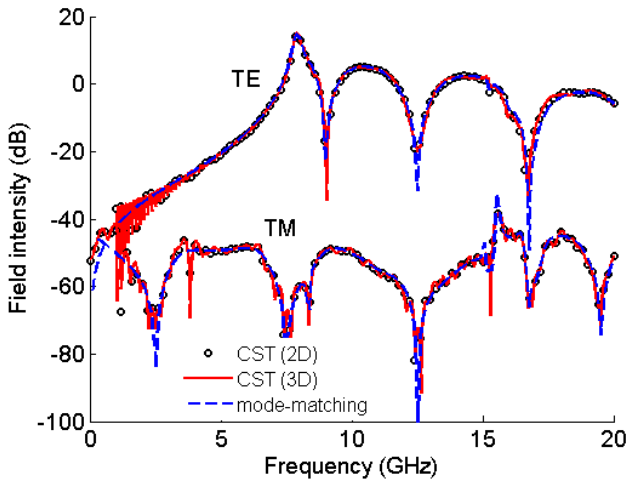


Fig. 3. Comparison of modelling results; now considering the field inside the structure at $[x; y; z] = [11 \text{ cm}; 0 \text{ cm}; -2 \text{ cm}]$.

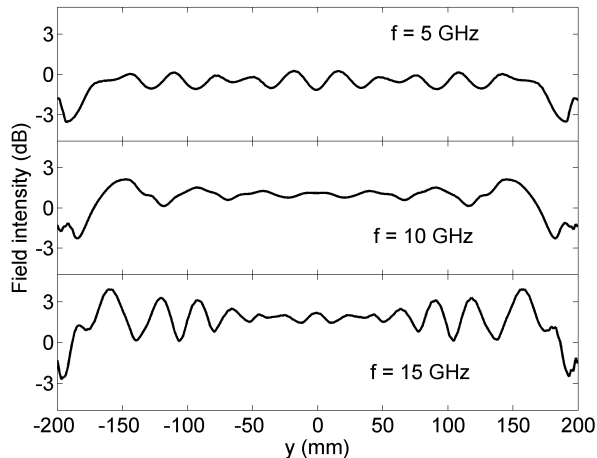


Fig. 4. Field amplitude as a function of y ($x = 11 \text{ cm}$, $z = 0 \text{ cm}$) for TE-polarized wave and for three distinct frequencies 5 GHz, 10 GHz and 15 GHz.

The CST simulated E-field intensity on the boundary of the two regions as a function of y -dimension ($x = 11 \text{ cm}$, $z = 0 \text{ cm}$) is shown in Fig. 4 documenting that the field along the y -axis can be considered roughly invariant.

As well as obtaining accurate results for the examples given in this paper, the analytical mode-matching method several orders of magnitude faster than CST. For example, for a computer with a 2.83 GHz processor and 8 GB RAM, the mode matching technique takes 200 ms to analyze the structure for one polarization and 200 frequency points as shown in Figs 2 and 3. The calculation of the same result using CST takes approximately 10 minutes for the 3D case and approximately 60 seconds for the 2D case.

B. Comparison of analytical results with CST for combs with a thickness greater than zero

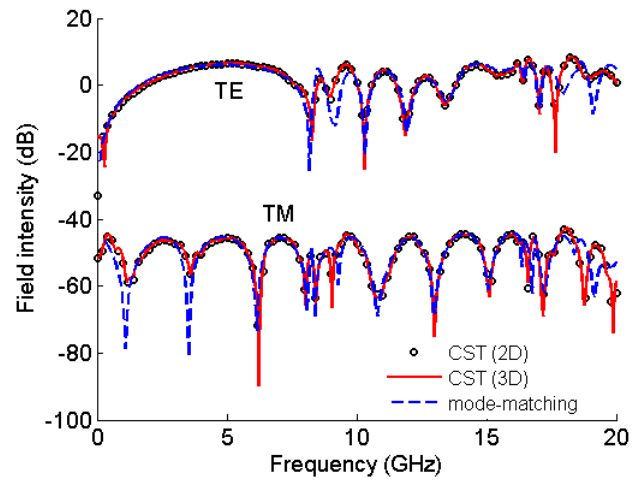


Fig. 5. Comparison of modelling results; considering the field on the boundary of the Region I and Region II, $[x; y; z] = [11 \text{ cm}; 0 \text{ cm}; 2 \text{ cm}]$. For a thickness, $t = 1.6 \text{ mm}$

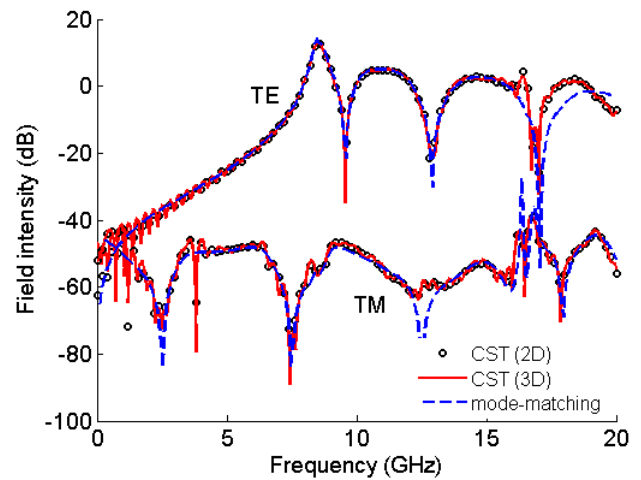


Fig. 6. Comparison of modelling results; field on the boundary of the Region I and Region II, $[x; y; z] = [11 \text{ cm}; 0 \text{ cm}; -2 \text{ cm}]$. For a thickness, $t = 1.6 \text{ mm}$

Numerical simulations and the proposed analytical technique are compared for fins of non-zero thickness is shown in Figs. 5 and 6 for surfaces with a thickness of 1.6 mm. The results show there is still a good agreement between the proposed approach

based on mode matching and the fully numerical solution by CST for non-zero thickness. Increased fin thickness lowers the separation of the plates of the waveguide formed by the fins and shifts the frequency pattern in Figs. 5 and 6 towards higher frequencies compared to the case of infinitely thin fins. This applies only to TE polarization, however. For TM polarization the fin thickness is not significant.

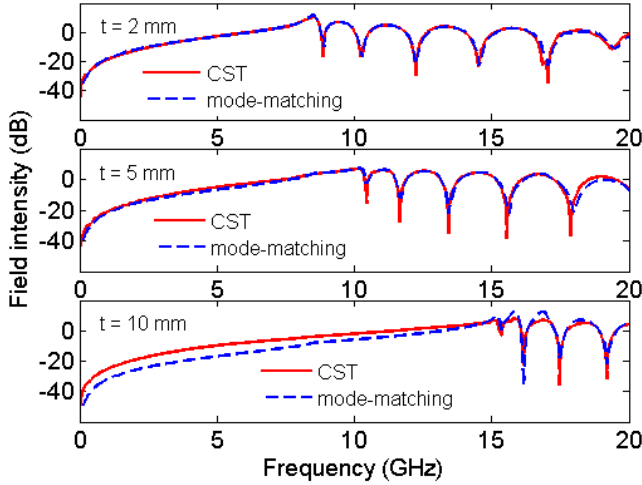


Fig. 7a. Comparison of modelling results for TE polarization; field on the boundary of the Region I and Region II, $[x; y; z] = [11 \text{ cm } 0 \text{ cm } 0 \text{ cm}]$. Thickness t varies from 2.0 mm to 10 mm as indicated.

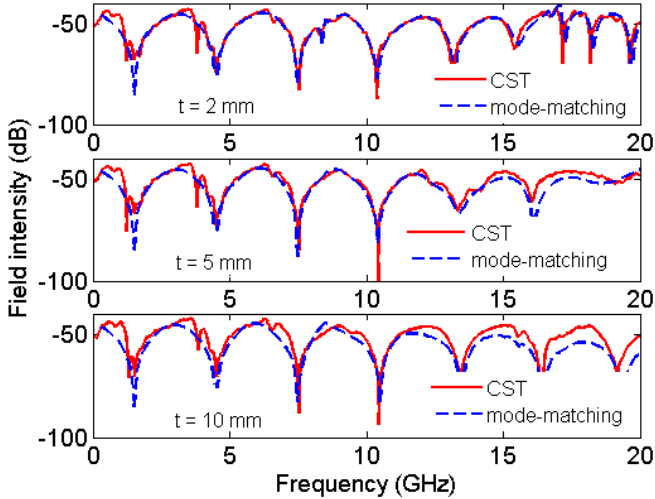


Fig. 7b. Comparison of modelling results for TM polarization; field on the boundary of the Region I and Region II, $[x; y; z] = [11 \text{ cm } 0 \text{ cm } 0 \text{ cm}]$. Thickness t varies from 2.0 mm to 10 mm as indicated.

To investigate the influence of the fin thickness t on the

mode-matching simulation accuracy, comparisons have been made for three cases ($t = 2 \text{ mm}$, $t = 5 \text{ mm}$ and $t = 10 \text{ mm}$) while keeping the fins' period constant ($p = 20 \text{ mm}$). The resulting comparisons can be seen in Fig. 7a and 7b for TE and TM polarization, respectively. It can be observed that the two results correspond quite well for smaller fin thickness (where $t/p \leq 0.25$) while diverging for increased fin thickness (where $t/p = 0.5$).

IV. FAR-FIELD SCATTERING FOR INFINITELY THIN COMBS

In order to calculate the far-field scattering by the periodic surface with infinitely thin combs, the scattered component of the field $\psi^I(x, y)$ has to be calculated at points where $z=0$ and integrated over the surface of the structure using Kirchhoff-Huygens principle as [21]

$$E_s = \frac{jk_0}{4\pi r} \int_{-t}^X \int_{-W/2}^{W/2} \psi_s^I(x, 0) e^{jk_0 x \sin \phi} (\cos \theta + \cos \phi) dy dx \quad (12)$$

where

$$\psi_s^I(x, z) = \sum_{m=-\infty}^{\infty} A_m e^{-j(\alpha_m x + \beta_m z)} \quad (13)$$

and where the exponential term in (12) represents the phase shift relative to an element at $x=0$. The phase term $e^{-jk_0 r}$ is neglected in (12). W is the width of the structure measured along the y -axis and X is the dimension of the structure along the x -axis which can be expressed as $X = (N_f - 1) \cdot p$ where N_f is the number of fins and p is the fin period. The distance, r is the distance between the surface and the receiving point, and is the same for all points on the structure due to the far-field scattering assumption. Evaluating (12) gives the far-field scattering at a distance r in the x - z plane as a function of incidence, θ and scattering angle, ϕ .

$$E_s = \frac{k_0 W (\cos \theta + \cos \phi)}{4\pi r} \sum_{m=-\infty}^{\infty} A_m \frac{e^{-j(\alpha_m - k_0 \sin \phi) X} - 1}{k_0 \sin \phi - \alpha_m} \quad (14)$$

Fig. 8 shows the far-field scattering pattern of the structure as a function of scattering angle, ϕ at a frequency of 12 GHz. In this case, the fins of the structure are infinitely thin. The angle of incidence, θ is 50° . In this case, the reference distance for the pattern calculation was 1 m. relatively good agreement can be observed between the CST prediction and mode matching simulation using (14). Our mode matching equations offer a good prediction of the expected CST result in a much faster

$$E_s^{TE} = \frac{k_0 W}{4\pi r} (\cos \theta + \cos \phi) \sum_{n=0}^{N_f-2} \sum_{m=-\infty}^{\infty} \frac{A_m e^{j(k_0 \sin \phi - \alpha_m) np}}{k_0 \sin \phi - \alpha_m} [e^{j(k_0 \sin \phi - \alpha_m) L} - 1] \quad (15)$$

$$E_s^{TM} = \frac{k_0 W}{4\pi r} (\cos \theta + \cos \phi) \left(\sum_{n=0}^{N_f-2} \sum_{m=-\infty}^{\infty} \frac{A_m e^{j(k_0 \sin \phi - \alpha_m) np}}{k_0 \sin \phi - \alpha_m} [e^{j(k_0 \sin \phi - \alpha_m) L} - 1] - \sum_{n=0}^{N_f-1} \frac{e^{jk_0 (\sin \phi - \sin \theta) np}}{k_0 (\sin \phi - \sin \theta)} [1 - e^{-jk_0 (\sin \phi - \sin \theta) t}] \right) \quad (16)$$

solver time, with small discretion for $\phi > 75^\circ$ and $\phi < -55^\circ$ for TE and TM polarization.

V. FAR-FIELD SCATTERING FOR COMBS WITH A THICKNESS GREATER THAN ZERO

A similar approach as in Section IV was used to derive formulas analogical to (14) for a structure with fins of a thickness greater than zero. Note that the amplitude of $\psi_s^I(x, 0)$ is equal to zero and one for $n(L + t) - t < x < n(L + t)$ in the case of TE and TM polarization, respectively, due to boundary conditions; $n = 0, 1, \dots, N_f - 1$. Evaluating (12) and taking into account boundary conditions gives equations (15, 16). Fig. 9 shows the far-field scattering pattern of the structure as a function of scattering angle, ϕ . The periodic structure is the same as in the previous case with exception of thickness of the fins set equal to $t = 1.6$ mm.

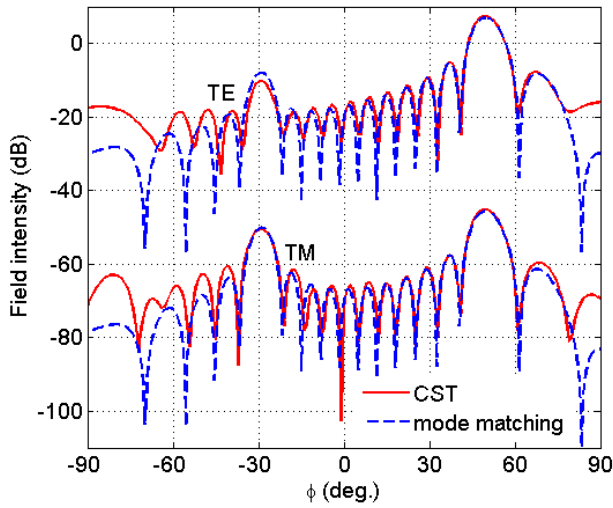


Fig. 8. Comparison of CST modelling results and mode matching formula using equation (10). The far-field scattering pattern for an angle of incidence, $\theta = 50^\circ$ for $t = 0$ mm at a frequency of 12 GHz.

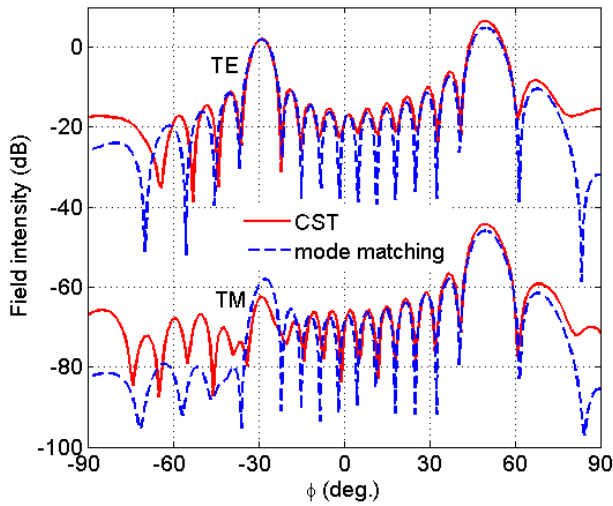


Fig. 9. Comparison of CST modelling results and mode matching formula using equation (10). The far-field scattering pattern for an angle of incidence, $\theta = 50^\circ$ for $t = 1.6$ mm at a frequency of 12 GHz.

The frequency of interest is 12 GHz. As can be seen from comparison of Figs. 8 and 9, the fin thickness has an impact on the scattering pattern.

VI. EXPERIMENTAL MEASUREMENT OF FAR-FIELD CHARACTERISTICS

Further investigation of the far-field characteristics was conducted using CST simulations, the mode-matching method, and retrospective far-field scattering measurements. To perform accurate measurements for comparison and validation of the other two techniques, a prototype aluminum surface was manufactured using bent aluminum strips secured using rivets to an aluminum ground plane, creating a surface with overall dimensions of 621×600 mm. The constructed surface had a fin period of 23 mm, height of 50 mm, and thickness of 1.6 mm. The final prototype is shown in Fig. 10.

Measurements of the aluminum surface were conducted to characterize the far-field scattering of the surface, relative to angle of scatter. These were conducted in a bi-static measurement chamber, developed in [22]. A frequency range of 8 to 18 GHz was measured, using a sweep time of 2 seconds, and intermediate frequency bandwidth (IFBW) of 1 KHz on an Agilent E8720 vector network analyzer (VNA). Relevant time gates were used to remove noise.



Fig. 10. The constructed aluminum surface, with a fin period of 23 mm, height of 50 mm, and thickness of 1.6 mm. The surface has 27 repetitions of fins secured on a ground plane of 621×600 mm.

A. Far-field measurements at 12 GHz

The scattering from the periodic aluminum prototype and a flat metal plate were measured for both TM and TE polarization, and plots at 12 GHz are shown in Figs. 11 and 12 respectively. For TM polarization, there is a clear reduction in specular scatter at 50° , redirected as backscatter at approximately -20° . Due to the large beamwidth of the horn antenna, the peak in specular scatter covers a large angle of scatter than in CST simulations and mode-matching solutions. A similar response is shown for TE polarization in Fig. 12, although the surface does not have such a large reduction in specular scatter at this frequency for TE polarization. Once again, there is a peak increase in backscatter at -20° .

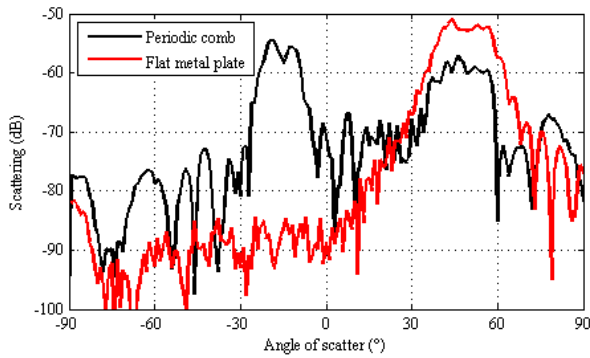


Fig. 11. The far-field scattering pattern for TM polarization at a frequency of 12 GHz, comparing results from the periodic comb and flat plate.

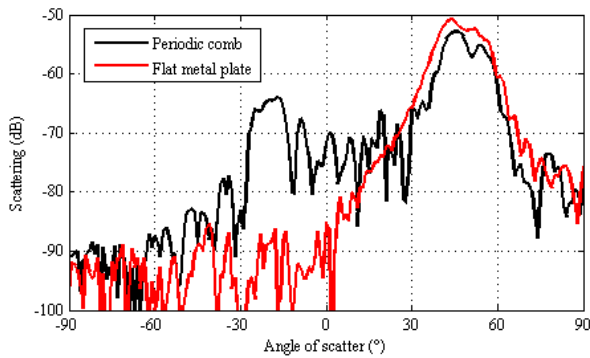


Fig. 12. The far-field scattering pattern for TE polarization at a frequency of 12 GHz, comparing results from the periodic comb and flat plate.

B. Full scattering analysis

Measurement results were extended to produce a scattering measurement across a whole range of frequencies for comparison with both CST simulations and mode-matching results. This was done for TM polarisation and an angle of incidence of 50° .

A full frequency sweep of the scattering characteristics using the bi-static measurement system is shown in Fig. 13. The main scattering lobes can be compared to Figs. 14, where a similar response is obtained using the mode matching technique, whilst illuminated with a unitary amplitude plane wave and receiver reference distance equal to 1 meter. For both cases it is possible to see the sweeping backscatter angle as the frequency increases. As previously described in literature this is linked to Bragg's Law [4, 22]. The beamwidth in Fig. 13 is much larger due to the types of antenna horn used in measurement.

Simulation results of the CST model in Fig. 15 reveal an identical response to that Fig. 14, showing that the mode-matching technique can be used to accurately obtain results much more quickly than measurements and numerical techniques.

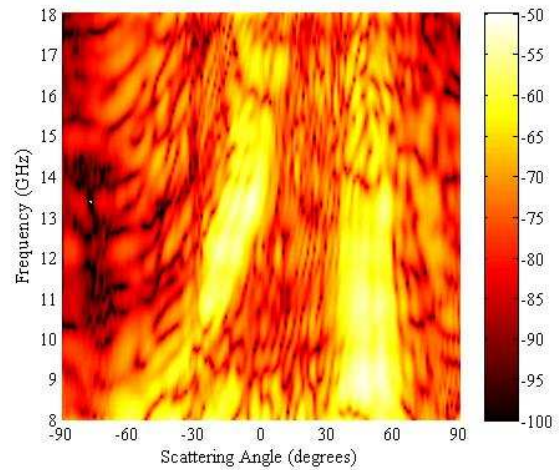


Fig. 13. The measured scattering magnitude for a frequency of 8 GHz and 18 GHz between scattering angles of -90° and 90° for TM polarization.

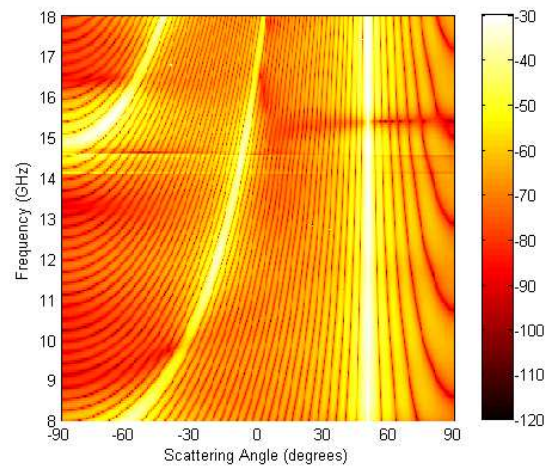


Fig. 14. The mode matching scattering magnitude for a frequency of 8 GHz and 18 GHz between scattering angles of -90° and 90° for TM polarization.

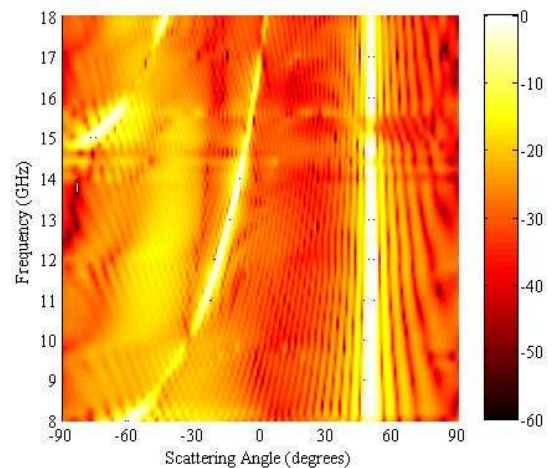


Fig. 15. CST simulation plot of the scattering magnitude for a frequency of 8 GHz and 18 GHz between scattering angles of -90° and 90° for TM polarization.

VII. CONCLUSIONS

In this work we have presented a novel mode-matching technique that is suitable for calculating the electric and magnetic fields within the near-field region of a periodic comb surface and the resultant far-field scattering pattern. The fields can be expressed as an infinite sum of modes and the coefficients of individual modes are obtained by solving the proposed set of linear equations. The proposed technique is suitable for analysis of such surfaces illuminated by both E-polarized and H-polarized incident waves. Analysis has been performed for two cases where the comb thickness is either infinitely thin or of a finite thickness. Calculated results are in good agreement to those obtained using the finite integration techniques (FIT) implemented in CST Microwave Studio (CST MSW). Our mode matching technique is computational faster by several orders of magnitude when compared to FIT. Furthermore, numerical results are compared to measurements of an aluminum prototype. Far-field scattering measurements are obtained using a bi-static system. These results provide additional confidence in the validity of CST simulations and the mode matching methods presented within this paper.

REFERENCES

- [1] A. Thain, J. P. Estienne, J. Robert, G. Peres, G. Cambon, L. Evain and B. Spitz, "A solution for ILS disturbance due to a building," in European Conf. on Antennas and Propagation (EuCAP), Prague, Czech Rep., 2012, pp. 2392–2395.
- [2] H. Kapasi, J. Blackburn and C. Mias, "The use of corrugated surfaces to improve wireless signal strength in the shadow region of buildings," *Microw. and Opt. Techn. Lett.*, vol. 46, no. 5, pp. 467–469, Sept., 2005.
- [3] C. J. Davenport, J. M. Rigelsford, J. Zhang and H. Altan, "Periodic comb reflection frequency selective surface for interference reduction," in Antennas and Propag. Conf. (LAPC), Loughborough, UK, 2013, pp. 615–618.
- [4] C. J. Davenport and J. M. Rigelsford, "Specular Reflection Reduction using Periodic Frequency Selective Surfaces," *IEEE Trans. Antennas Propagat.*, vol. 62, no. 9, pp. 4518–4527, 2014.
- [5] T. J. Park and H. J. Eom, "TE-scattering and reception by a parallel-plate waveguide array," *IEEE Trans. Antennas Propagat.*, vol. 42, no. 6, pp. 862–865, June 1994.
- [6] G. A. Kriegsmann and B. J. McCartin, "Scattering by a rectangular corrugated surface: an approximate theory," *IEEE Trans. Antennas Propagat.*, vol. 44, no. 8, pp. 1193–1194, Aug. 1996.
- [7] E. E. Kriezis and D. P. Chrissoulidis, "EM-wave scattering by an inclined strip grating," *IEEE Trans. Antennas Propagat.*, vol. 41, no. 11, pp. 1473–1480, Nov. 1993.
- [8] P. Valtr and P. Pechac, "Closed-form approximation for parallel-plate waveguide coefficients," *Radioengineering*, vol. 22, no. 4, pp. 1296–1300, Dec. 2013.
- [9] J. L. Uretsky, "The scattering of plane waves from periodic surfaces," *Ann. Phys.*, vol. 33, pp. 400–427, 1965.
- [10] P. M. van den Berg, "Diffraction theory of a reflection grating," *Appl. Sci. Res.*, vol. 24, pp. 261–293, July 1971.
- [11] E. V. Jull and G. Ebbeson, "The reduction of interference from large reflecting surfaces," *IEEE Trans. Antennas Propagat.*, vol. 25, no. 4, pp. 565–570, July 1977.
- [12] S.-L. Chuang and J. A. Kong, "Scattering of Waves from Periodic Surfaces," *Proceedings of the IEEE*, vol. 69, no. 9, pp. 1132–1144, Sept. 1981.
- [13] R. I. Masel, R. P. Merrill and W. H. Miller, "Quantum scattering from a sinusoidal hard wall: Atomic diffraction from solid surfaces," *Phys. Rev. B*, vol. 12, pp. 5545–5551, 1975.
- [14] J. A. DeSanto, "Scattering from a sinusoid: Derivation of linear equations for the field amplitudes," *J. Acoust. Soc. Amer.*, vol. 57, pp. 1195–1197, 1975.

- [15] P. C. Waterman, "Scattering by periodic surface," *J. Acoust. Soc. Amer.*, vol. 57, pp. 791–802, 1975.
- [16] A. I. Papadopoulos and D. P. Chrissoulidis, "EM wave scattering by a dihedral strip grating," *Antennas and Propagation Society International Symposium*, vol. 1, pp. 102–106, June 1993.
- [17] R.-B. Hwang, "Scattering Characteristics of Plane Wave by a 1D Periodic Structure Consisting of a Cavities Array," in *Periodic Structures: Mode-Matching Approach and Applications in Electromagnetic Engineering*, 1st ed. Singapore, Singapore: John Wiley & Sons, 2013, ch. 6, sec. 1, pp. 246–255.
- [18] S. Tretyakov, "Periodical structures, arrays, and meshes," in *Analytical Modeling in Applied Electromagnetics*, Norwood: Artech House, 2003, ch. 4, pp. 69–118.
- [19] G. James, "Green's theorem in a plane", in *Advanced Modern Engineering Mathematics*, 3rd ed. Edinburgh, Scotland, Pearson, 2004, ch. 7, sec. 4, pp. 570.
- [20] Computer Simulation Technology (CST), [Online]. Available: <http://www.cst.com/Content/Products/MWS/Overview.aspx>.
- [21] H. L. Bertoni, "Diffraction by edges and corners," in *Radio Propagation for Modern Wireless Systems*, New Jersey: Prentice Hall, 2000, ch. 5, pp. 107–139.
- [22] C.J. Davenport and J. M. Rigelsford, "Novel indoor bi-static measurement facility for full scattering characterisation of surfaces at oblique incidence," *Journal of Electromagnetic Waves and Applications*, vol. 28. no. 14, pp. 1798–1806, 2014.



Pavel Valtr received his Ing. (M.Sc.) and Ph.D. degrees both in Radio Electronics from the Czech Technical University in Prague, Czech Republic, in 2004 and 2007, respectively.

From 2007 to 2009 he was a Research Fellow at the University of Vigo, Vigo, Spain working on various topics in electromagnetic wave propagation including rough surface and vegetation scattering and land mobile satellite channel modeling. In 2009 he joined the European Space Agency (ESA/ESTEC), Noordwijk, The Netherlands as a Post-Doctoral Research Fellow. Since 2012 he has been with the Czech Technical University in Prague as a Researcher. His research interests include wireless and satellite communications and computational methods in electromagnetics.

Dr. Valtr received the Young Scientist Award of XXVIII General Assembly of the International Union of Radio Science (URSI) in 2005.



Christopher J. Davenport received the M.Eng. degree in Electrical Engineering from the University of Sheffield, Sheffield, UK in 2010.

He has been studying for the PhD degree at the Department of Electronic and Electrical Engineering at the University of Sheffield, since 2011. His current research interests include periodic frequency selective surfaces (FSS), implantable RFID, and active FSS.

Mr Davenport was co-recipient of the 2nd place award at Loughborough Antennas and Propagation Conference (LAPC) for Best Non-Student Paper in 2013.



Pavel Pechac received the M.Sc. degree and the Ph.D. degree in Radio Electronics from the Czech Technical University in Prague, Czech Republic, in 1993 and 1999 respectively. He is currently a Professor at the Department of Electromagnetic Field, Czech Technical University in Prague. His research interests are in the field of radiowave propagation and wireless systems.



Jonathan M. Rigelsford (SM'13) received the MEng and PhD degrees in Electronic Engineering from the University of Hull, Hull, UK in 1997 and 2001 respectively.

From 2000 to 2002, he worked as Senior Design Engineer at Jaybeam Limited, designing antennas for cellular base stations. From late 2002, until 2014 he was a Senior Experimental Officer for the Communications Group within the Department of Electronic and Electrical Engineering, University of Sheffield, Sheffield, UK. He is now a Senior Research Fellow at the same institution.

Dr Rigelsford has been an active member of the Antenna Interface Standards Group (AISG) from 2002 to 2010 being elected to the board of directors during that time. More recently, he has become Secretary to the Wireless Friendly Building Forum, an industrial/academic initiative to promote understanding of radio propagation within the built environments.

His current research interests include RF propagation, adaptive antennas, RFID and cyber security.